LETTERS

The rate of N-WASP exchange limits the extent of ARP2/3-complex-dependent actin-based motility

Ina Weisswange[1], Timothy P. Newsome[1]†, Sibylle Schleich[1] & Michael Way[1]

Understanding cell motility will require detailed knowledge not only of the localization of signalling networks regulating actin polymerization, but also of their dynamics. Unfortunately, many signalling networks are not amenable to such analysis, as they are frequently transient and dispersed. By contrast, the signalling pathways used by pathogens undergoing actin-based motility are highly localized and operate in a constitutive fashion[1–5]. Taking advantage of this, we have analysed the dynamics of neuronal Wiskott–Aldrich syndrome protein (N-WASP), WASP-interacting protein (WIP), GRB2 and NCK, which are required to stimulate actin-related protein (ARP)2/3-complex-dependent actin-based motility of vaccinia virus[6–9], using fluorescence recovery after photobleaching. Here we show that all four proteins are rapidly exchanging, albeit at different rates, and that the turnover of N-WASP depends on its ability to stimulate ARP2/3-complex-mediated actin polymerization. Conversely, disruption of the interaction of N-WASP with GRB2 and/or the barbed ends of actin filaments increases its exchange rate and results in a faster rate of virus movement. We suggest that the exchange rate of N-WASP controls the rate of ARP2/3-complex-dependent actin-based motility by regulating the extent of actin polymerization by antagonizing filament capping.

During infection, vaccinia virus enhances its cell-to-cell spread by stimulating ARP2/3-complex-dependent actin polymerization beneath the extracellular enveloped virus by locally activating Src- and Abl-dependent signalling cascades[6,10–12] consisting of GRB2, NCK, WIP and N-WASP[6–9,13] (Fig. 1a). To obtain insights into the dynamics of this signalling network, we examined the turnover rates of green fluorescent protein (GFP)-tagged GRB2, NCK, WIP and N-WASP recruited to the tips of virus-induced actin tails (Fig. 1b and Supplementary Figs 1, 2), using fluorescence recovery after photobleaching (FRAP). We found that all four GFP-tagged proteins rapidly recover to nearly pre-bleach values, suggesting that they do not form a stable complex beneath the virus (Fig. 1c and Supplementary Fig. 3). Similar results were also observed for GFP-tagged NCK and N-WASP in cell lines lacking endogenous NCK or N-WASP (Supplementary Figs 2, 3). Unexpectedly, the recovery of N-WASP is ~3.5 times slower than that of NCK and WIP, although they are thought to be responsible for the recruitment of N-WASP[6–8,13]. The similar recovery rates of NCK and WIP suggest that these proteins may be functioning together as a complex. However, NCK is still recruited by the virus independently of WIP in N-WASP-null cells (Fig. 1d, e). Our data suggest that WIP and N-WASP are recruited to the virus as a complex in a NCK-dependent fashion.

Our previous observations indicate that the recruitment of GRB2, which is dependent on phosphorylation of tyrosine 132 of A36R and the presence of N-WASP (Fig. 1a, d), results in the formation of more actin tails than in its absence[9]. To determine whether GRB2 promotes actin tail formation by stabilizing the actin tail-nucleating complex, we examined the exchange rate of NCK, WIP and N-WASP, which are recruited to actin tails in the absence of tyrosine-132 phosphorylation (Fig. 2a). The A36R–Y132F virus, which does not recruit GRB2, formed fewer actin tails than the Western Reserve (WR) strain (Supplementary Fig. 4). Moreover, FRAP analyses reveal that the absence of GRB2 results in a significant increase in the rate of recovery, not only of N-WASP but also NCK and WIP (Fig. 2b, c and Supplementary Figs 4, 5). A role for GRB2 in stabilization of the complex is also consistent with the increased rate of recovery of GFP–NCK in the absence of GRB2, WIP and N-WASP recruitment in N-WASP-null cells (Fig. 1e and Supplementary Fig. 3).

To confirm our observations obtained using the A36R–Y132F virus, we examined the effects of RNA interference (RNAi)-mediated depletion of GRB2. FRAP analyses on RNAi-treated cells reveal that loss of GRB2 also increases the rates of recovery for NCK, WIP and N-WASP (Fig. 2d, e and Supplementary Fig. 5). These effects are specific to the loss of GRB2, as expressing cyan fluorescent protein (CFP)–GRB2-res, which is resistant to RNAi, results in NCK, WIP and N-WASP exchange rates that are similar to the control values (Fig. 2d, e and Supplementary Fig. 5). Taken together, our data show that GRB2 is acting as a secondary adaptor to help stabilize the vaccinia actin-tail-nucleating complex.

Even in the absence of GRB2, the rate of recovery of N-WASP did not approach that of NCK or WIP. One possible explanation is that N-WASP is stabilized by an additional interaction. Recent observations have shown that the WASP-homology 2 (WH2) domains of N-WASP, or actin bound to these domains, can interact with free barbed ends of growing actin filaments[14]. To test whether this interaction might explain why N-WASP turns over more slowly than NCK and WIP, we expressed GFP-tagged N-WASP–R410A/R438A (RA/RA), which has a 30-fold-lower affinity for actin monomers than the wild-type protein[14], in N-WASP-null cells (Fig. 3a and Supplementary Fig. 6). N-WASP-null cells expressing GFP–N-WASP–RA/RA that were infected with WR or A36R–Y132F viruses had significantly fewer actin tails than those complemented with N-WASP (Supplementary Fig. 6). The loss of GRB2 recruitment and/or N-WASP–RA/RA also resulted in significantly shorter actin tails (Fig. 3b and Supplementary Fig. 6). FRAP analysis revealed that N-WASP–RA/RA has a faster exchange rate than N-WASP in WR-infected cells (Fig. 3c, d and Supplementary Fig. 6). Interactions between WH2 and actin thus help to stabilize N-WASP during ARP2/3-complex-mediated actin polymerization. However, this interaction cannot explain why the dynamics of N-WASP–RA/RA is slower than that of NCK and WIP even in the absence of GRB2.

We therefore wondered whether an interaction between N-WASP and the ARP2/3 complex responsible for nucleating actin polymerization

[1]Cell Motility Laboratory, Cancer Research UK, London Research Institute, 44 Lincoln's Inn Fields, London WC2A 3PX, UK. †Present address: School of Molecular and Microbial Biosciences, G08 - Biochemistry and Microbiology, University of Sydney, New South Wales 2006, Australia.

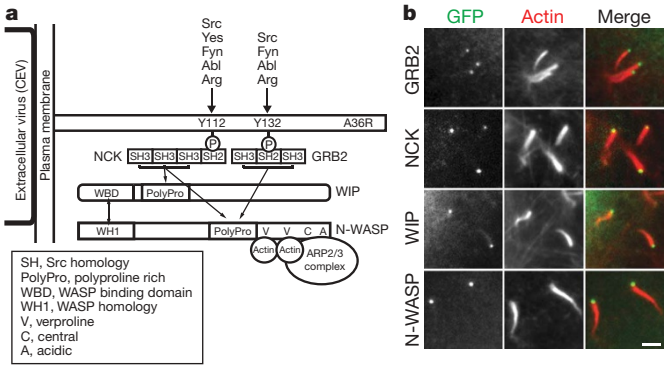

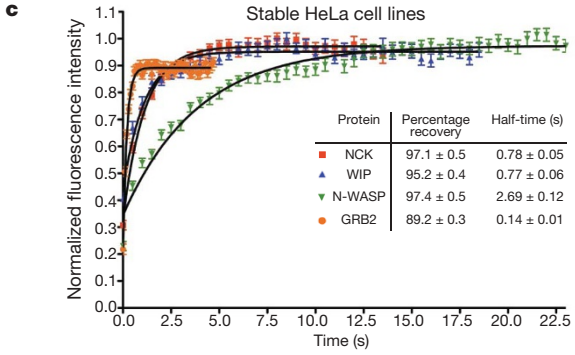

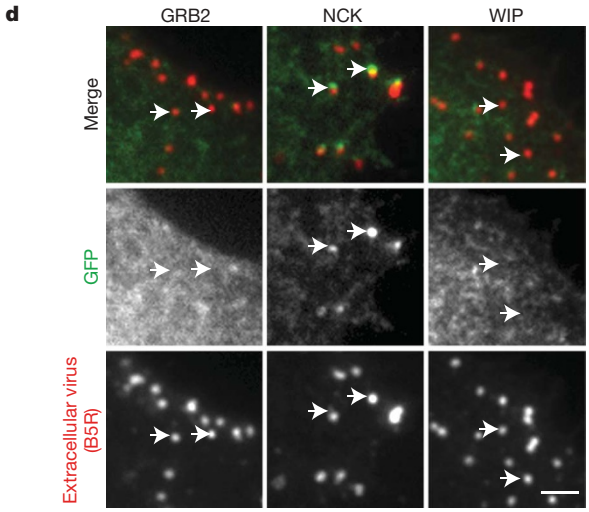

e

GFP–NCK in N-WASP-null cells

Virus	Percentage recovery	Half-time (s)
WR	96.9 ± 0.3	0.49 ± 0.02
A36R–Y132F	98.2 ± 0.3	0.48 ± 0.02

Figure 1 | Components of the vaccinia actin-nucleating complex are highly dynamic. **a**, Sketch indicating the interactions between the proteins recruited beneath extracellular virus particles that are responsible for stimulating ARP2/3-mediated actin tail formation. Src- and Abl-family kinases known to phosphorylate tyrosine 112 or 132 of A36R are indicated together with motifs and domains. **b**, Immunofluorescence images demonstrating that GFP-tagged NCK, GRB2, WIP and N-WASP (green) are recruited to the tips of virus-induced actin tails (red) in infected HeLa cells. Scale bar, 2.5 μm. **c**, The recovery kinetics of the indicated GFP-tagged protein on the tips of actin tails after photobleaching. Error bars, s.e.m. with $n = 52$. The values for the percentage and half-time of recovery for each protein are indicated. **d**, GFP-tagged NCK, but not GRB2 or WIP, is recruited beneath extracellular virus particles (B5R, red) in N-WASP-null cells. Scale bar, 2.5 μm. **e**, Values derived from 52 fitted recovery curves together with the s.e.m. for the percentage and half-time of recovery of GFP–NCK in N-WASP-null cells infected with the indicated virus.

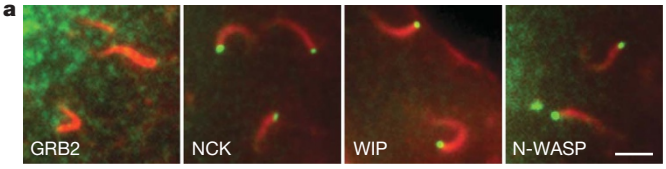

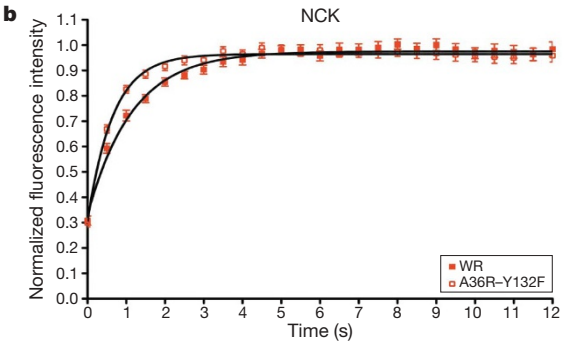

c

Stable HeLa cells		WR	A36R–Y132F
NCK	Percentage recovery	97.5 ± 0.5	96.5 ± 0.4
	Half-time (s)	0.8 ± 0.05	0.45 ± 0.03***
WIP	Percentage recovery	95.2 ± 0.4	95.6 ± 0.4
	Half-time (s)	0.76 ± 0.06	0.35 ± 0.03***
N-WASP	Percentage recovery	97.4 ± 0.5	95.4 ± 0.6
	Half-time (s)	2.68 ± 0.01	1.72 ± 0.03***

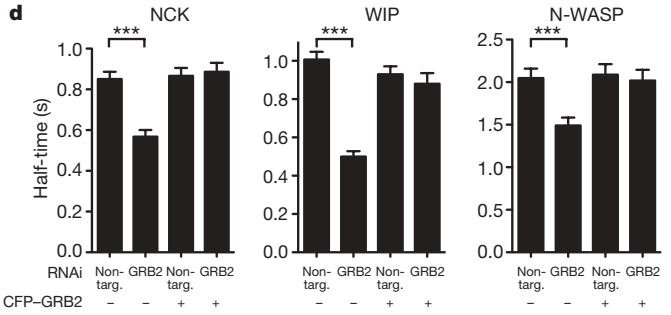

e

RNAi		Non-targ.	GRB2	Non-targ.	GRB2
CFP–GRB2		–	–	+	+
NCK	Percentage recovery	97.9 ± 0.4	99.7 ± 0.4	98.2 ± 0.4	100 ± 0.5
	Half-time (s)	0.85 ± 0.04	0.56 ± 0.03***	0.87 ± 0.04	0.88 ± 0.04
WIP	Percentage recovery	99.1 ± 0.4	97.4 ± 0.4	98.9 ± 0.5	99.4 ± 0.6
	Half-time (s)	1 ± 0.03	0.5 ± 0.03***	0.93 ± 0.04	0.87 ± 0.06
N-WASP	Percentage recovery	96.2 ± 0.7	96.4 ± 0.8	95.1 ± 0.8	96.1 ± 0.8
	Half-time (s)	2.05 ± 0.11	1.47 ± 0.93***	2.09 ± 0.12	2.03 ± 0.13

Figure 2 | GRB2 stabilizes the vaccinia actin-nucleating complex. **a**, Immunofluorescence images demonstrating that GFP-tagged NCK, WIP and N-WASP, but not GRB2, are recruited to the tips of actin tails induced by the A36R–Y132F virus. Scale bar, 2.5 μm. **b**, The recovery kinetics of GFP–NCK on the tips of actin tails after photobleaching in WR- and A36R–Y132F-infected HeLa cells. Error bars, s.e.m.; $n = 52$. **c**, Values derived from 52 fitted recovery curves for the percentage and half-time of recovery together with the s.e.m. of the indicated GFP-tagged protein in HeLa cells infected with WR and A36R–Y132F viruses. **d**, The half-time of recovery of GFP-tagged NCK, WIP and N-WASP on the tips of actin tails in HeLa cells treated with the indicated RNAi, GRB2-specific or non-targeting control (non-targ.), with or without expression of RNAi-resistant CFP–GRB2. Error bars, s.e.m.; $n = 52$. **e**, Values derived from 52 fitted recovery curves together with the s.e.m. of the percentage and half-time of recovery for the indicated GFP-tagged proteins in HeLa cells treated with the indicated RNAi. ***$P < 0.001$.

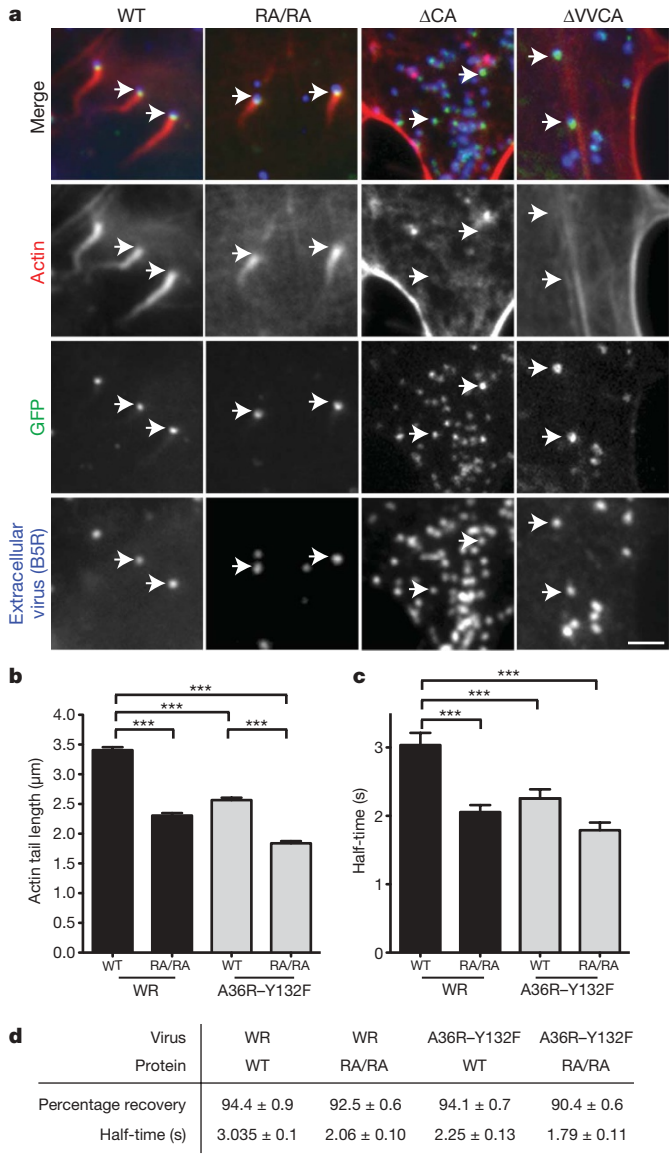

d

Virus	WR	WR	A36R–Y132F	A36R–Y132F
Protein	WT	RA/RA	WT	RA/RA
Percentage recovery	94.4 ± 0.9	92.5 ± 0.6	94.1 ± 0.7	90.4 ± 0.6
Half-time (s)	3.035 ± 0.1	2.06 ± 0.10	2.25 ± 0.13	1.79 ± 0.11

Figure 3 | WH2:actin filament interactions contribute to N-WASP stability. a, Immunofluorescence images demonstrating that GFP-tagged wild-type (WT), RA/RA, ΔCA and ΔVVCA N-WASP are recruited beneath extracellular virus particles (B5R, blue) in the N-WASP-null cells. Only GFP-tagged N-WASP and RA/RA mutant are able to rescue actin tail formation (red) in the N-WASP-null cells. Scale bar, 2.5 μm. **b**, The length of actin tails induced by WR and A36R–Y132F viruses in rescued N-WASP-null cells expressing GFP-tagged N-WASP or N-WASP–RA/RA. Error bars, s.e.m. with $n = 450$. **c**, The half-time of recovery of GFP-tagged N-WASP and N-WASP–RA/RA in WR- and A36R–Y132F-infected cells. Error bars, s.e.m. with $n = 52$. **d**, Values derived from 52 fitted recovery curves together with the s.e.m. for GFP-tagged N-WASP or N-WASP–RA/RA in N-WASP-null cells infected with the indicated virus. $^{***}P < 0.001$.

might also contribute to its stability. The turnover rate of N-WASP with WH2, central and acidic regions deleted, N-WASP–ΔVVCA, which is unable to promote ARP2/3-complex-dependent actin tail formation, was examined (Fig. 1a)[7]. GFP–N-WASP–ΔVVCA was recruited beneath virus particles but was unable to promote their movement, as it cannot stimulate actin tail formation in N-WASP-null cells (Fig. 3a and Supplementary Fig. 6). Unexpectedly, we found that after bleaching, GFP–N-WASP–ΔVVCA did not recover (Fig. 4a and Supplementary Fig. 7). GFP–N-WASP with central and acidic regions deleted, GFP–N-WASP–ΔCA, which can still bind actin monomers but is unable to interact with the ARP2/3 complex, was also recruited beneath the virus and did not turn over (Figs 3a and 4a).

The lack of recovery of these mutants would suggest that the turnover of N-WASP is dependent on active actin polymerization. We therefore examined the turnover rate of N-WASP in the presence of cytochalasin D, a potent inhibitor of actin polymerization[15]. Cytochalasin D inhibited actin tail formation and virus movement, although GRB2, NCK, WIP and N-WASP were still recruited (Fig. 4b, data not shown and Supplementary Fig. 8). The ARP2/3 complex (anti-ARPC5) and actin were also still recruited to the virus, albeit at reduced levels in the presence of the drug (Supplementary Fig. 9). Moreover, the recovery of GFP-tagged N-WASP and WIP was severely reduced (Fig. 4c and Supplementary Fig. 8). By contrast, NCK was able to recover, albeit at a slower rate, consistent with its ability to be recruited independently of WIP and N-WASP. The turnover rate of GRB2 remained essentially unchanged (Fig. 4c). One possible explanation for our observations is that interaction of N-WASP with the ARP2/3 complex and stimulation of actin polymerization promotes its dissociation from WIP. This dissociation would allow both proteins to act independently of each other, consistent with their different rates of exchange.

An actin filament nucleated by the ARP2/3 complex will polymerize until a capping protein blocks the growing barbed end. An interaction of the growing barbed end with the WH2 domains of N-WASP would also effectively limit filament extension. The association of N-WASP with the barbed end of a growing actin filament as well as the ARP2/3 complex nucleating a new actin filament could explain why N-WASP has a slower exchange rate than NCK and WIP. Ultimately however, this interaction may limit the overall rate of virus movement, as it competes with the addition of actin monomers to the growing barbed end of filaments beneath the virus. The turnover of N-WASP is therefore required for actin-based motility of the virus, and at the same time active actin polymerization is required to promote turnover of the molecule. This hypothesis is consistent with recent observations demonstrating that release of N-WASP from actin and the ARP2/3 complex is required for actin-based motility of functionalized giant unilamellar vesicles[16].

Our model predicts that the stability of N-WASP beneath the virus, which is dependent on GRB2 and active actin polymerization, will determine how fast the virus moves, as it will regulate the overall rate of actin polymerization in the actin tail. To examine if this is the case, we measured the rate of actin-based virus movement in the absence of GRB2 and in cells only expressing N-WASP–RA/RA (Fig. 4d). We found that loss of the stabilizing influence of GRB2 on N-WASP results in significantly faster rate of movement for the A36R–Y132F virus ($0.33 \pm 0.01\ \mu m\ s^{-1}$ versus $0.28 \pm 0.01\ \mu m\ s^{-1}$). Disruption of the interaction of N-WASP with the barbed end of actin filaments also promoted a similar increase in speed ($0.34 \pm 0.01\ \mu m\ s^{-1}$). An increase in the rate of movement of lipid-coated beads is also observed in *in vitro* motility assays when the WH2 domains of N-WASP are disrupted[14]. The fastest rate of virus movement ($0.37 \pm 0.01\ \mu m\ s^{-1}$) was observed in A36R–Y132F-infected cells only expressing N-WASP–RA/RA (Fig. 4d).

Our results indicate that the reduced stability of N-WASP enhances virus motility even though the actin tails get shorter (Fig. 3b). The formation of shorter tails suggests that reducing N-WASP-barbed end interactions does not actually lead to more extensive growth of individual actin filaments. It could, however, result in increased capping of barbed ends by capping proteins because of reduced competition with N-WASP beneath the virus. Consistent with this, previous observations in reconstituted *in vitro* motility assays have shown that increased capping of barbed ends also increases the rate of *Listeria* motility, although actin tail lengths get shorter[17]. Our suggestion is further supported by recent observations demonstrating that capping protein enhances actin-based motility by promoting actin filament nucleation by the ARP2/3 complex[18].

In conclusion, we suggest that in the steady state, it is the stability of N-WASP association beneath the extracellular virus that determines how fast it moves, by virtue of its ability to regulate actin

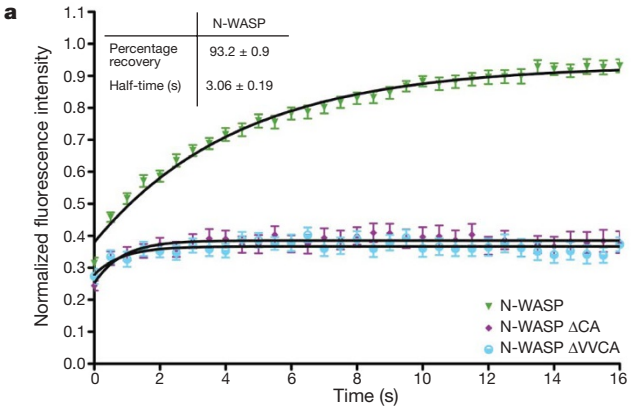

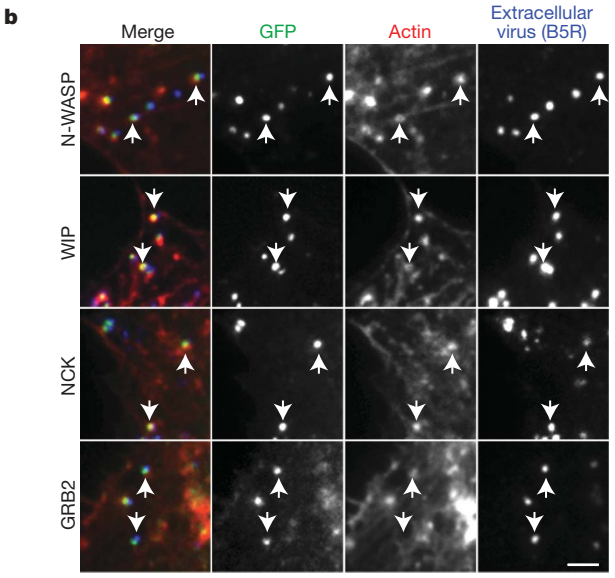

c

	GRB2		NCK		WIP		N-WASP	
	Untreated	Cyto D	Untreated	Cyto D	Untreated	Cyto D	Untreated	Cyto D
Percentage recovery	87.2 ± 0.4	85 ± 0.3	100.7 ± 0.4	97.9 ± 0.3	100 ± 0.4	56.2 ± 0.5	96.8 ± 0.7	67.6 ± 0.9
Half-time (s)	0.1 ± 0.006	0.12 ± 0.006	0.82 ± 0.04	1.84 ± 0.06	0.93 ± 0.05	1.84 ± 0.21	1.92 ± 0.09	2.88 ± 0.27

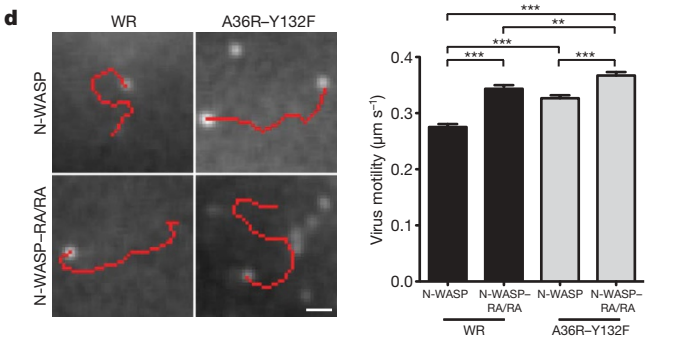

Figure 4 | Virus movement and N-WASP turnover is dependent on actin polymerization. a, The recovery kinetics of GFP-tagged N-WASP, ΔCA and ΔVVCA after photobleaching, together with the fitted data for N-WASP. Error bars, s.e.m. with $n = 52$. **b**, GFP-tagged NCK, GRB2, WIP and N-WASP are recruited by extracellular virus particles (B5R, blue) but are unable to induce actin tails in the presence of cytochalasin D. Scale bar, 2.5 μm. **c**, The percentage and half-time of recovery derived from 52 fitted recovery curves for the indicated proteins in the presence or absence of cytochalasin D (cyto D). **d**, Images illustrating the movement of WR and A36R–Y132F viruses over 1 min (red line) in N-WASP-null cells expressing GFP-tagged N-WASP or N-WASP–RA/RA. Scale bar, 1 μm. The graph shows the average speed of virus movements ($n = 120$–150) over 1 min. $^{**}P < 0.01$, $^{***}P < 0.001$.

filament growth by antagonizing capping proteins. Furthermore, the inverse relationship between the rate of N-WASP exchange and the number of actin tails suggests that there is also a critical balance between the stability of N-WASP, barbed-end capping and ARP2/3-complex-dependent actin filament nucleation. Future studies will be aimed at understanding the relationship between these parameters as well as the organization of filaments within virus-induced actin tails.

METHODS SUMMARY

Cell lines, infection and immunofluorescence. Stable cell lines expressing GFP-tagged GRB2, NCK1, WIP, N-WASP and N-WASP mutants were created using recombinant lentiviruses and isolated by fluorescence-activated cell sorting (FACS) as described previously[19]. Cells were infected with WR and A36R–Y132F strains of vaccinia virus and processed for immunofluorescence analysis to reveal extracellular virus particles, the actin cytoskeleton and GFP signals as described previously[20]. Actin tail formation was quantified as previously described[9].

Live cell imaging and FRAP analysis. Live cell imaging of vaccinia-infected cells at 37 °C was performed using a Plan-Apochromat ×63/1.4 objective on a Zeiss Axiovert 200 equipped with a Photometrics Cascade II camera controlled by Metamorph. The motion of the GFP–N-WASP signal associated with 120–150 red fluorescent protein (RFP)-tagged viruses at the tip of actin tails was tracked for 1 min using Metamorph to calculate the average speed in micrometres per second.

All FRAP experiments were performed using a Zeiss LSM 510 META system with a Plan-Apochromat ×63/1.4 objective at 37 °C. The GFP signal associated with moving virus particles was bleached using two iterations of the 488-nm laser at 80% power followed by image acquisition every 300 ms (except in the case of GRB2, where there was no delay) with laser power settings of 4% for 488 nm (GFP) and 8% for 568 nm (RFP) using an open pinhole. The recovery of the GFP signal associated with the virus was measured using Metamorph. The resulting background-subtracted data was then normalized to the first pre-bleached image and fitted using the Prism software and the equation $Y_{(t)} = (Y_{max} - Y_{min})(1 - e^{-kt}) + Y_{min}$ (ref. 21), where $Y_{(t)}$ is the intensity of fluorescence at time t, Y_{max} and Y_{min} are respectively the maximum and minimum intensities of fluorescence post-bleaching and k is the rate constant of recovery. In all cases, the percentage, the rate constant and the half-time of recovery were derived from 52 fitted recovery curves together with the s.e.m. and significance where appropriate.

Full Methods and any associated references are available in the online version of the paper at www.nature.com/nature.

Received 23 October 2008; accepted 12 January 2009.

1. Frischknecht, F. & Way, M. Surfing pathogens and the lessons learned for actin polymerization. *Trends Cell Biol.* **11**, 30–38 (2001).
2. Munter, S., Way, M. & Frischknecht, F. Signaling during pathogen infection. *Sci. STKE* **2006**, doi: 10.1126/stke.3352006re5 (2006).
3. Bhavsar, A. P., Guttman, J. A. & Finlay, B. B. Manipulation of host-cell pathways by bacterial pathogens. *Nature* **449**, 827–834 (2007).
4. Pawson, T. & Warner, N. Oncogenic re-wiring of cellular signaling pathways. *Oncogene* **26**, 1268–1275 (2007).
5. Backert, S., Feller, S. M. & Wessler, S. Emerging roles of Abl family tyrosine kinases in microbial pathogenesis. *Trends Biochem. Sci.* **33**, 80–90 (2008).
6. Frischknecht, F. *et al.* Actin based motility of vaccinia virus mimics receptor tyrosine kinase signalling. *Nature* **401**, 926–929 (1999).
7. Moreau, V. *et al.* A complex of N-WASP and WIP integrates signalling cascades that lead to actin polymerization. *Nature Cell Biol.* **2**, 441–448 (2000).
8. Snapper, S. B. *et al.* N-WASP deficiency reveals distinct pathways for cell surface projections and microbial actin-based motility. *Nature Cell Biol.* **3**, 897–904 (2001).
9. Scaplehorn, N. *et al.* Grb2 and Nck act cooperatively to promote actin-based motility of vaccinia virus. *Curr. Biol.* **12**, 740–745 (2002).
10. Newsome, T. P., Scaplehorn, N. & Way, M. SRC mediates a switch from microtubule- to actin-based motility of vaccinia virus. *Science* **306**, 124–129 (2004).
11. Reeves, P. M. *et al.* Disabling poxvirus pathogenesis by inhibition of Abl-family tyrosine kinases. *Nature Med.* **11**, 731–739 (2005).
12. Newsome, T. P., Weisswange, I., Frischknecht, F. & Way, M. Abl collaborates with Src family kinases to stimulate actin-based motility of vaccinia virus. *Cell. Microbiol.* **8**, 233–241 (2006).
13. Zettl, M. & Way, M. The WH1 and EVH1 domains of WASP and Ena/VASP family members bind distinct sequence motifs. *Curr. Biol.* **12**, 1617–1622 (2002).
14. Co, C., Wong, D. T., Gierke, S., Chang, V. & Taunton, J. Mechanism of actin network attachment to moving membranes: barbed end capture by N-WASP WH2 domains. *Cell* **128**, 901–913 (2007).

15. Kueh, H. Y., Charras, G. T., Mitchison, T. J. & Brieher, W. M. Actin disassembly by cofilin, coronin, and Aip1 occurs in bursts and is inhibited by barbed-end cappers. *J. Cell Biol.* **182,** 341–353 (2008).
16. Delatour, V. *et al.* Arp2/3 controls the motile behavior of N-WASP-functionalized GUVs and modulates N-WASP surface distribution by mediating transient links with actin filaments. *Biophys. J.* 94, 4890–4905 (2008).
17. Pantaloni, D., Boujemaa, R., Didry, D., Gounon, P. & Carlier, M.-F. The Arp2/3 complex branches filament barbed ends: functional antagonism with capping proteins. *Nature Cell Biol.* **2,** 385–391 (2000).
18. Akin, O. & Mullins, R. D. Capping protein increases the rate of actin-based motility by promoting filament nucleation by the Arp2/3 complex. *Cell* **133,** 841–851 (2008).
19. Arakawa, Y., Cordeiro, J. V. & Way, M. F11L-mediated inhibition of RhoA-mDia signaling stimulates microtubule dynamics during vaccinia virus infection. *Cell Host Microbe* **1,** 213–226 (2007).
20. Arakawa, Y., Cordeiro, J. V., Schleich, S., Newsome, T. & Way, M. The release of vaccinia virus from infected cells requires RhoA-mDia modulation of cortical actin. *Cell Host Microbe* **1,** 227–240 (2007).
21. Shewan, A. M. *et al.* Myosin 2 is a key Rho kinase target necessary for the local concentration of E-cadherin at cell-cell contacts. *Mol. Biol. Cell* **16,** 4531–4542 (2005).

Supplementary Information is linked to the online version of the paper at www.nature.com/nature.

Acknowledgements We would like to thank T. Pawson and S. Snapper for NCK- and N-WASP-null cell lines and the FACS laboratory (Cancer Research UK, London) for help sorting stable cell lines. We are also very grateful to the members of the Way laboratory, J. Beaudouin, M.-F. Carlier, H. Gerhardt, B. Mayer, K. Rottner, M. Rosen and M. Welch for discussions and comments on the manuscript. T.P.N. was funded in part by a fellowship from the Human Frontier Science Program (HFSP). This work was funded by Cancer Research UK.

Author Information Reprints and permissions information is available at www.nature.com/reprints. Correspondence and requests for materials should be addressed to M.W. (michael.way@cancer.org.uk).

METHODS

Generation of stable GFP cell lines and western-blot analysis. NCK $1/2^{-/-}$ (ref. 22) and N-WASP$^{-/-}$ (ref. 8) cells were provided by T. Pawson and S. Snapper, respectively. Inserts corresponding to GRB2, NCK, WIP, N-WASP and N-WASP–ΔVVCA were isolated from previously described vectors[6,7,9] and cloned into the Not1/EcoR1 site of a modified pLL3.7–GFP vector[19,23]. N-WASP–RA/RA and N-WASP-ΔCA mutants were created by PCR using GFP–N-WASP as a template. N-WASP–RA/RA and N-WASP–ΔCA were cloned into the Not1/EcoR1 sites of the pE/L–GFP and pLL3.7–GFP vectors. The fidelity of all clones was confirmed by sequencing.

Lentiviruses for each of the GFP-tagged proteins were produced using the Lentivirus system[19,23]. Cells were infected with lentiviruses and stable lines expressing the various GFP-tagged proteins isolated using FACS. The following cell lines expressing the indicated GFP-tagged protein were created: HeLa (GRB2, NCK, WIP and N-WASP); N-WASP$^{-/-}$ (N-WASP, N-WASP–ΔVVCA and N-WASP–ΔCA, and N-WASP–RA/RA) and NCK $1/2^{-/-}$ (NCK1).

Western-blot analysis of GFP-stable cell lines and short interfering RNA (siRNA)-treated cells was performed using the following primary antibodies: GFP 3E1 (Cancer Research UK); actin (Ac74), α-actinin (BM 7.52) and α-tubulin (DM14) (Sigma-Aldrich); NCK rabbit polyclonal (Upstate Biotech), GRB2 (81) (Transduction Laboratories); WIP (H224) (Santa Cruz) and N-WASP[7]. The following secondary antibodies were used: goat HRP conjugates to rabbit, rat and mouse IgG (Bio-Rad Laboratories).

Infections, immunofluorescence and actin tails. Cells were infected with WR or A36R–Y132F viruses at a multiplicity of infection of 0.5 and immunofluorescence analyses performed at 8 h post-infection for HeLa cells and 10 h post-infection for knockout cells as previously described[9,20]. Virus particles were labelled with an antibody against B5R (19C2 rat monoclonal)[24] and F-actin was stained using Alexa 568- or Alexa 488-phalloidin (Molecular Probes). The ARP2/3 complex was detected using anti-ARPC5 (p16-Arc) (323H3 mouse monoclonal, Synaptic Systems). Actin tail formation was quantified by counting 100 cells on three independent days as previously described[9]. Only B5R positive, that is, infected cells where virus particles had reached the cell periphery, were analysed. Actin tail length was assessed in N-WASP$^{-/-}$ cells stably expressing GFP–N-WASP or GFP–N-WASP–RA/RA 10 h after infection with WR or A36R–Y132F. The lengths of actin tails was determined from fixed images of ten individual cells in three independent experiments. For each of the four conditions, at least 450 actin tails were measured.

Construction of recombinant RFP–A3L vaccinia virus. A fragment of genomic WR DNA corresponding to 200 base pairs upstream of A3L was amplified by PCR and cloned into the KpnI site of pEL–RFP–A3L to create the targeting LA–RFP–A3L in pBS SKII. The RFP–A3L targeting vector was transfected into WR- and A36R–Y132F-infected cells. The viruses encoding RFP–A3L were isolated by successive rounds of plaque purification and the fidelity of the final recombinant viruses was confirmed by sequencing, immunofluorescence, plaque size comparison and re-infection assays as described previously[20].

Live-cell imaging, FRAP and data analysis. All live-cell imaging was performed on cells infected with WR and A36R–Y132F viruses that also encode RFP–A3L within their genome to ensure that the analysed GFP signal corresponds to a virus particle. Virus particle motility was analysed in N-WASP$^{-/-}$ cells stably expressing GFP-tagged N-WASP or N-WASP–RA/RA 10 h post-infection. The GFP signal was recorded every 5 s for a period of 3 min using a Plan-Apochromat 63/1.40 Oil Ph3 lens on a Zeiss Axiovert 200 equipped with a Cascade II (Photometrics) under the control of Metamorph (Molecular Devices). The motion of the GFP signal, which corresponds to the tip of an actin tail, was tracked using Metamorph over a period of 1 min to calculate the speed in micrometres per second. Imaging was performed on three independent days and more than 40 virus particles in at least ten different cells were analysed on each day.

All FRAP experiments were performed on a LSM 510 META system using a Plan-Apochromat 63/1.40 Oil Ph3 lens (Zeiss). Infected cells to be imaged were first identified under low-light fluorescence using the eyepiece. The particle to bleach was aligned live on the computer screen to a saved region of interest (ROI) for bleaching. Two pre-bleached images were acquired before the GFP signal was bleached using two iterations of the 488-nm laser at 80% power followed by acquisition of images with laser powers described above. Images were recorded with laser power settings of 4% for 488 nm (GFP) and 8% for 568 nm (RFP) using an open pinhole. The time interval between acquisitions was set to 300 ms, except in the case of GRB2, where there was no delay.

The fluorescence intensity of the bleached virus particle was determined using a fixed-size ROI, which was moved by hand to ensure it always remained centred over the moving virus particle, with Metamorph. The fluorescence intensity in a fixed ROI immediately adjacent to the virus was measured and an average value for the whole movie was subtracted from the virus signal to correct for background fluorescence. As the area imaged was small and virus particles were moving, it was not possible to correct for photo-damage because a reference non-bleached particle was not available in each movie. The resulting background-subtracted data was then normalized to the first pre-bleached image.

Kinetic modelling was performed using the Prism software and the equation $Y_{(t)} = (Y_{max} - Y_{min})(1 - e^{-kt}) + Y_{min}$ (ref. 21). The rate constant of recovery (k) and the maximum recovery compared with the first pre-bleached image (percentage recovery) were calculated from the fitted curves. The rate constant of recovery was used to calculate the half-time ($t_{1/2} = \ln 2/k$). Each curve represents an average of 52 virus particles that were acquired over three consecutive days in which between 15 and 20 viruses were bleached in at least five different cells. Data in the graphs are presented as mean and standard error of the mean.

RNAi treatments. HeLa cells were transfected with 20 pmol of a SMARTpool of four oligonucleotide duplexes against GRB2 (UGAAUGAGCUGGUGGAUUA UU, AGGCAGAGCUUAAUGGAAAUU, CGAAGAAUGUGAUCAGAACUU, GAAAGGAGCUUGCCACGGGUU) or the non-targeting SMARTpool 2 (Dharmacon) using the Lipofectamine RNAi Max kit (Invitrogen) according to the manufacturer's protocol. Two days post-transfection, cells were infected with WR and processed for FRAP analysis, immunofluorescence or western-blot analysis 8 h later. To rescue the RNAi effect on GRB2, an RNAi-resistant GRB2 was cloned Not/EcoR1 into the pE/L–CFP vector. The following primers were used to introduce silent mutations into the codons encoding the indicated amino acids in GRB2: Glu 30, Cys 32, Gln 34; Ala 39, Leu 41, Gly 43; Asn 129, Leu 131, Asp 133; Gly 196, Cys 198, His 199. The clone was verified by sequence analysis. RNAi-treated HeLa cells were infected with WR and transfected with the CFP–GRB2-res, which is resistant to RNAi, 4 h later using Effectine (Qiagen) according the manufacturer's protocol. Two hours post-transfection, cells were washed and allowed to recover for 2 h before imaging was started. Before analysing a cell the expression of CFP–GRB2-res in each cell was checked.

Cytochalasin D treatments. Cells were plated on fibronectin-coated coverslips or MatTek dishes to a confluency of around 70% the day before the experiment. Cells were infected for 8 h before cytochalasin D (Sigma-Aldrich) was added to the medium at a final concentration of 1 μM as described previously[20]. Cells were treated for 30 min before fixation or directly used for FRAP experiments.

Statistical analysis. The data in the graphs are presented as mean and standard error of the mean. The data were analysed by analysis of variance followed by Newman–Keuls multiple comparison test or Student's t-test using Prism 5.0 (GraphPad Software). Statistical analysis of fitted FRAP data was performed using the "Do the best fit values of selected parameters differ between data sets" function in Prism 5.0. A P value of <0.05 is considered statistically significant. A single asterisk indicates $P < 0.05$, a double asterisk indicates $P < 0.01$ and a triple asterisk indicates $P < 0.001$.

22. Bladt, F. *et al.* The murine Nck SH2/SH3 adaptors are important for the development of mesoderm-derived embryonic structures and for regulating the cellular actin network. *Mol. Cell. Biol.* **23,** 4586–4597 (2003).
23. Rubinson, D. A. *et al.* A lentivirus-based system to functionally silence genes in primary mammalian cells, stem cells and transgenic mice by RNA interference. *Nature Genet.* **33,** 401–406 (2003).
24. Hiller, G. & Weber, K. Golgi-derived membranes that contain an acylated viral polypeptide are used for vaccinia virus envelopment. *J. Virol.* **55,** 651–659 (1985).